Review

Not peer-reviewed version

A review on performance and stability improvement of ternary semi-transparent organic solar cells: Material and architectural approaches

Peshawa O. Amin , Fahmi F. Muhammadsharif * , Salah Raza Saeed , Kamal Aziz Ketuly

Posted Date: 10 July 2023

doi: 10.20944/preprints202307.0522.v1

Keywords: Bulk heterojunction, ternary active layer, semitransparent OSCs, natural dyes

Review

A Review on Performance and Stability Improvement of Ternary Semi-Transparent Organic Solar Cells: Material and Architectural Approaches

Peshawa O. Amin [1], Fahmi F. Muhammadsharif [2,*], Salah Raza Saeed [3], Kamal Aziz Ketuly [4]

[1] Chrmo Center for Research, Training and Consultancy, Charmo University, 46023 Chamchamal, Kurdistan Region, Iraq; peshawa.amin@charmouniversity.org
[2] Department of Physics, Faculty of Science and Health, Koya University, Koya KOY45, Kurdistan Region - F.R., Iraq; fahmi982@gmail.com
[3] Advanced Polymeric Materials Research Lab., Department of Physics, College of Science, University of Sulaimani, Qlyasan Street, Sulaimani 46001, Iraq; salah.raza@univsul.edu.iq
[4] Department of Medical Chemistry, College of Medicine, University of Duhok, Duhok, Kurditan Region, Iraq; kketuly@yahoo.com
* Correspondence: fahmi982@gmail.com

Abstract: In the past decade, considerable efforts have been devoted to the development of semitransparent organic solar cells. Numerous materials and architectures have been proposed for the future commercialization of these devices. Among these, the use of ternary active layers demonstrated a great promise for the development of efficient semi-transparent organic solar cells with the potential for future applications including self-powered greenhouses and powered windows. Researchers seek alternative solutions to the trade-off between device power conversion efficiency (PCE) and average visible transmittance (AVT), with photoactive materials being the key parameters that govern both (PCE) and (AVT) as well as device stability. Several new organic materials, including polymers and small molecules, were synthesized, and used in conjunction with a variety of techniques to achieve semitransparent conditions. In this review paper, we will look at the working principle and key parameters of semi-transparent organic solar cells, as well as the methods that have been used to improve the performance of ternary-based semi-transparent organic solar cells. The main approaches were concluded to be spectral enhancement and transparency increment of the active layer through bandgap tuning, utilizing novel organic semiconductors, and design architecture of the active layers.

Keywords: Bulk heterojunction; ternary active layer; semitransparent OSCs; natural dyes

1. Introduction

In recent decades, people have been especially concerned about pollution from energy sources and greenhouse gases. To reduce these effects, many countries have put money and effort into the field of renewable energy. Among the renewable energy sources, solar energy is the most affordable, unpolluted and abundant of all long-term natural resources up to date [1]. Solar photovoltaic devices are among the most efficient means of turning sunlight into direct current in solar cells [2]. Solar cell technologies can be classified into organic and inorganic based semiconductors [3]. In the present day, silicon-based solar cells have been commercialized and have grown to dominate solar cell technology, despite limitations that have hampered the device's efficiency, such as poor absorption in the long wavelength range, cost-effectiveness, and highly complex fabrication procedures. Furthermore, the thickness and bandgap of the devices active layer has a vital role in modifying the optical and electrical properties of photovoltaic devices. For instance, thick films absorb more of the sun spectrum and form photo-generated carriers, but due to the likelihood of recombination, it is difficult to collect these carriers [4,5].

Organic/polymer solar cells (OSCs) were chosen as a viable alternative for photovoltaic applications. This is because polymer solar cells (PSCs) draw a vast interest due to their low cost, easy fabrication, transparency, flexibility, and capability of fine-tuning of bandgap energy. For highly

 doi:10.20944/preprints202307.0522.v1

efficient solar cells, conjugated polymers were used as a raw material in the active layer of polymer solar cells with a bulk heterojunction (BHJ) structure. In addition, polymer solar cells have proven to be a practical and cost-effective solar cell for portable electronic devices and building-integrated photovoltaic devices [6–8]. Nevertheless, due to intrinsic and extrinsic factors, stability and efficiency have not reached the benchmark for commercialization. Several significant endeavors have been done to improve stability and efficiency by means of modifying their active materials and device architecture [9–11]. One of the accomplishments to improve power conversion efficiency (PCE) while preserving flexibility, easy fabrication and low cost is the ternary system for bulk heterojunction active layer. The binary system's narrow window of absorption spectra of organic materials reduces device efficiency, whereas the ternary system improves light harvesting by broadening the spectral response of the active layer. Hence, this approach enhances the short circuit current density (J_{sc}) and film morphology, and as a result the device performance is amended.

A ternary system comprises a combination of two donors and an acceptor, or a donor and two acceptors, or a donor and an acceptor with a third component such as small molecules or dyes. Therefore, selecting the third components is a remarkable consideration for device performance. The third component determines the mechanism of charge transfer and compatibility of film morphology, which have a direct impact on the device efficiency and stability [12–14].

The ability of organic materials to tune their bandgap energy revealed a new field of practices for niche applications of building-integrated photovoltaics (PVs), such as self-powered greenhouses and powered windows, known as semi-transparent organic photovoltaics (ST-OPV). Despite the fact that ST-OPV has not yet been commercialised, the trade-off between device efficiency and average visible transparency (AVT) remains a challenge, and a number of researchers have assigned their research to increasing the efficiency to a commercial standard and optimising (AVT) as well [15–18]. A review of the literature showed that there were useful reviews on ternary systems for bulk heterojunction structure [19–28], as well as several interesting reviews on the progress of semi-transparent organic solar cells from materials to device performance [29–35]. For a semi-transparent organic solar cell, several parameters should be taken into consideration, such as film thickness, active layer materials, and electrodes. This means that semi-transparent solar cells and ternary blend systems rely heavily on optical tuning of the active layer materials to facilitate such adjustments [36–39]. Semi-transparent organic solar cells have undergone significant development in recent years, and this review paper provides a thorough examination of the photovoltaic parameters of these cells, as well as an elaboration on the latest advancements, approaches, and active layer conditions that have contributed to this growth.

2. Working Mechanism of Ternary Organic Solar Cells

Organic solar cells (OSCs) are photovoltaic devices that use organic semiconductors in their active layer to convert solar energy into electricity. π-conjugated backbone of carbon-based materials are the supreme organic semiconductors for light harvesting. These materials are defined by the frontier molecular orbitals formed by a parallel overlapping of π bonds. The uppermost π band is known as the highest occupied molecular orbitals (HOMO), whereas the lowermost π^* denotes the lowest unoccupied molecular orbital (LUMO). The optical energy band gap is the difference between the HOMO and LUMO levels that determines the material's optical characteristics. Because of the absorption of electromagnetic radiation, excitons (e-h pairs) are generated. As a result of the low dielectric constant (ε_r) around 2-4 and the existence of many localized states in the photo excited state, the mutual Coulomb interaction between e-h pairs will be in the range of 0.3-1 eV (see Figure 1).

Preprints (www.preprints.org) | NOT PEER-REVIEWED | Posted: 10 July 2023 doi:10.20944/preprints202307.0522.v1

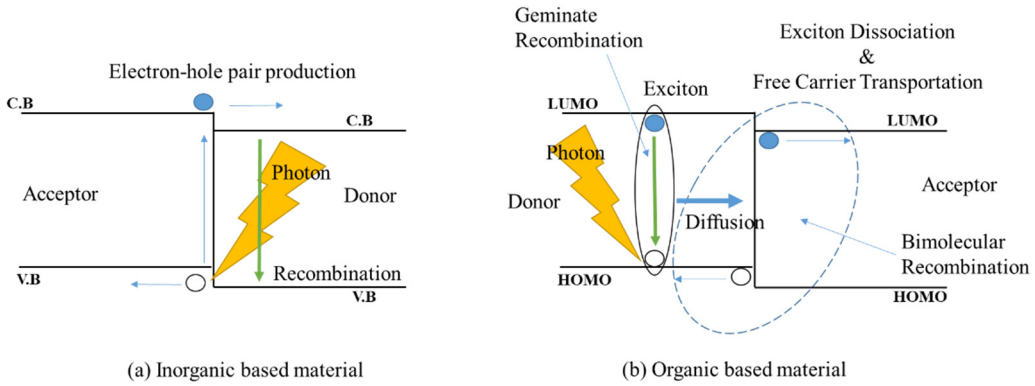

Figure 1. The process of photocurrent generation in (**a**) Inorganic materials, and (**b**) Organic materials (authors created illustration).

Excitons have a binding energy that is larger than the thermal energy present at ambient temperature, therefore extra energy is needed to dissociate singlet excitons and generate sufficient free charges in the active layer. As a result, a crucial strategy for overcoming the binding energy of excitons and detaching electrons and holes is a heterojunction structure, which comprises of an electron-donating (donor) and electron-accepting (acceptor) materials. The driving energies for exciton dissociations are provided because of the differences in ionization energy of the materials which leads to generate an energy offset at the interfaces. Incidentally, excitons must travel to the interface for dissociation process, whereas the organic materials possess a localized nature at excited states, so the excitons travel by random diffusion. This is because excitons are electrically neutral and hence unaffected by an electric field. However, the random diffusion process incoherently derived by both Dexter energy transfer and Förster resonance energy transfer (FRET) are taken place intramolecularly or intermolecularly. As a result, singlet excitons experience a short lifetime in the excited state. Therefore, the diffusion length of excitons is short of around 5-20 nm. Consequently, a thin layer is advantageous for excitons to extend to the interfaces without decaying to ground state [29,40].

Consequently, it is vital to analyse a trade-off between photon absorption and exciton dissociation in relation to semiconductors. Bulk heterojunction (BHJ) was introduced by Heeger's group to overcome the short diffusion length of exciton, low charge mobility and weak absorption rate. The BHJ is composed of a mixture of donor and acceptor elements. As previously stated, enlarging the interfacial area is a critical mechanism for excitons dissociation, so any photoinduced excitons appear to be a few nanometres away from the donor-acceptor interface at any point in the interpenetrating network. Figure 2 depicts a schematic illustration of photocurrent generation and the architecture of a bulk heterojunction organic solar cell. Charge generation and transport in the BHJ organic solar active layer may be summarised as follows: i) Excitons are created when photons are absorbed in the donor region. ii) Excitons diffuse towards the interface of donor and acceptor moieties, where they dissociate into free charges. iii) Free carriers pass through the acceptor and donor domains in opposite direction. iv) The free charges are collected by the anode and cathode electrodes, respectively.

Preprints (www.preprints.org) | NOT PEER-REVIEWED | Posted: 10 July 2023 doi:10.20944/preprints202307.0522.v1

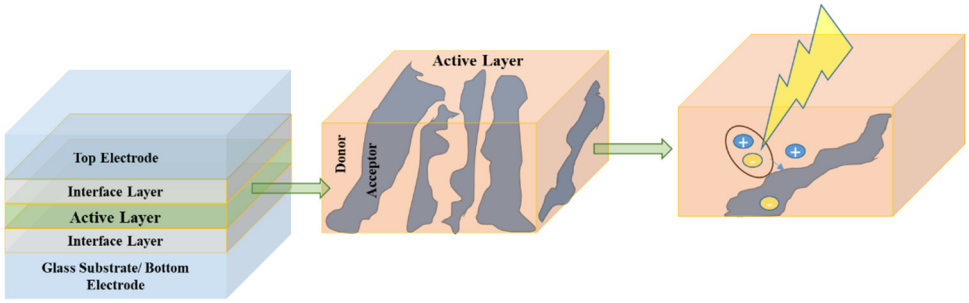

Figure 2. Schematic illustration of the architecture and photocurrent generation of BHJ organic solar cell (authors created illustration).

To attain the exceptional device performance of the BHJ structure, the absorption efficiency of the active layer, particularly the film thickness, must be enhanced. Most of the organic semiconductors have a low charge mobility, and for efficient charge transportation and collection, the typical thickness of the active layer is about 100 nm. Based on the Beer–Lambert law, as shown in Equation 1 [37], the absorption response is in a direct relation with the film thickness.

$$\boldsymbol{A = c\varepsilon d} \quad (1)$$

Where A is the absorbance, c is concentration of solution, ε is the molar absorptivity, and d is the optical path length (thickness of the active layer). To strike a balance between absorption efficiency and charge extraction, a novel design of organic solar cell called ternary organic solar cell (TOSC) was developed. This design can improve the morphology of the active layer, the device's stability, the recombination rate, and the voltage loss. In the ternary approach, the active layer consists of the blending of three components: a donor (D) and an acceptor (A) as a host binary material, plus an additional donor or acceptor. This strategy preserves the solution's processability and large-scale production, which is a step toward commercialisation [19].

The materials used in the BHJ structure were categorized based on their structure, including polymers, small molecules, nanostructures, and dyes. Therefore, selecting the third component in a ternary system induces more convolution in the charge transport mechanism, whereas the contribution of third components enhances all absorption profile, exciton dissociation, charge transport, and film morphology. The literature shows that the mechanism of charge transport in ternary systems involves four main operative mechanisms. The transport mechanism involves the energy levels and band gaps of the three components, entitled charge transfer and energy transfer mechanisms, whereas parallel like and alloy models rely on the nanomorphology of the active layer. Due to the placement of inserted components in the ternary active layer, it is remarkable that in some systems, more than one mechanism may exist simultaneously [19,25]. Thus, the location of the third component has a decisive role in defining the transport mechanism of charge carriers, as shown in Figure 3.

Preprints (www.preprints.org) | NOT PEER-REVIEWED | Posted: 10 July 2023 doi:10.20944/preprints202307.0522.v1

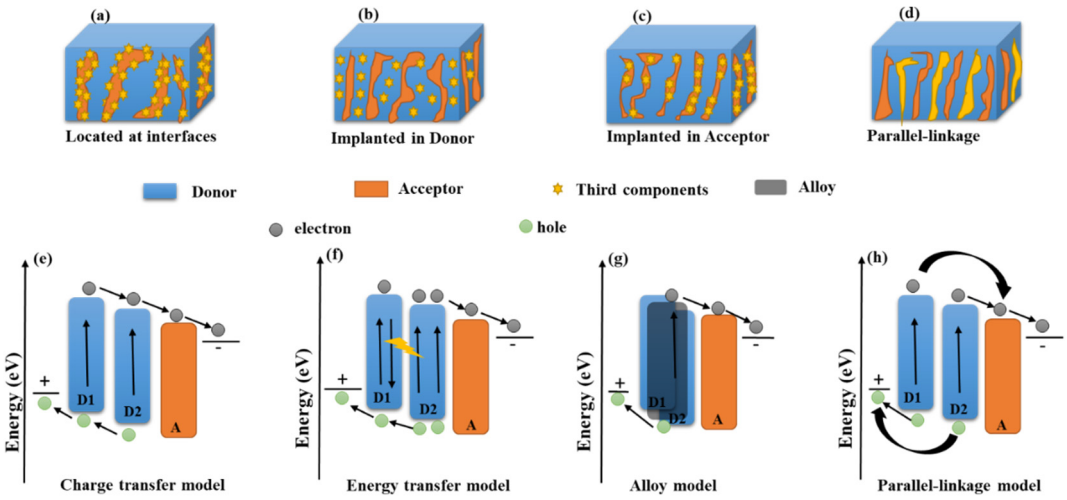

Figure 3. (**a**–**d**) Possible locations of the third component in ternary active layer, (**e**–**h**) Transport mechanisms for charge carriers in ternary organic solar cells (authors created illustration).

In the charge transport mechanism, photogenerated excitons at both donors (D1-D2-A ternary system) split apart at the interfaces between donors and acceptors, and electrons and holes are moved along the energy cascades toward their respective electrodes. For charge transport to occur, there are several crucial factors. First, the electronic energy levels of the three components must form an energy cascade alignment, as described in Figure 3e. In choosing the third component, whether it's small molecules or dyes, you should think about its energy levels (HOMO and LUMO) to avoid traps and excitons recombination in the active layer. Hence, it is located between the energy levels of the host binary system. Second, the position of the third component must be located at the interfaces of the host binary system (Figure 3a) and this depends on the crystallinity and the surface energy of the host materials [41,42]. Finally, the weight ratio of the third component has a strong influence on the type of charge transport, and in this model, the binary domains, which act as mediums for free carriers, should be conserved. To retain these routes in the binary domain and avoid disruption, a significant augmentation of the third component is required [43,44].

Energy transport mechanisms are another comprehend transport mechanisms that take place in ternary systems, as shown in Figure 3f. The third component acts as an absorber for harvesting more photons and transferring the energy of excited electrons to the host binary system. This energy exchange between the third component and host materials has been done through two main transfer mechanisms called Förster resonance energy transfer (FRET) and Dexter energy transfer (DET). In FRET, the electrons are excited to excited state through absorption process and bound to the nuclei of the molecules. The electrons do not transfer to other molecules, whereas their energy exchanges with the host materials via dipole-dipole interaction significantly depend on spectral overlap and intermolecular distance. However, in DET, electron exchange occurs at a short distance between molecules via a hoping process caused by molecular orbital overlaps. The position of the third component is then an essential feature due to the short intermolecular distance criterion for energy transfer.

As shown in Figure 3b,c, the third component should be in contact with a binary host material (Donor or Acceptor) to ensure efficient energy transfer and dissociation of excitons [22,23,45]. As a result, various experimental techniques were used to categorise and distinguish the type of charge dynamics within ternary systems, and photoluminescence measurement (PL) was chosen as a convenient technique to distinguish between charge and energy transfer. As a result, the charge transfer occurs if the emission intensity of the host materials (donor or acceptor) is quenched by entering the third component. However, if the emission intensity of the host donor gradually drops while the emission intensity of the host accepter steadily increases, this implies that energy transfer happens [22,23]. Nevertheless, due to experimental conditions such as film thickness, molecular alignment, and measuring angles, some unavoidable errors are produced. Hence, additional

Preprints (www.preprints.org) | NOT PEER-REVIEWED | Posted: 10 July 2023 doi:10.20944/preprints202307.0522.v1

techniques are used for determining the type of charge transfer. For instance, transient absorption (TA) spectroscopy and steady-state photoinduced absorption (PIA) were employed to probe charge dynamics [41,46].

Street and Yang proposed a new model for charge transport in BHJ solar cells called the alloy and parallel-linkage models, respectively. As shown in Figure 3g, in the alloy model, the two donors merged, acting as one donor, and due to comparable electronic properties, and a quasi-LUMO and quasi-HOMO energy level were formed. Moreover, at the charge transfer state, the electrons from alloy donors are transported through the percolating pathway of the accepter and holes through the percolating pathway of alloy donors towards the respective electrodes. For efficient transfer, the third component should have a good miscibility and compatibility with respect to the host materials. Nonetheless, in the parallel linkage model (Figure 3h), the two donors do not merge to form an alloy but individually contribute to charge transfer states. Thus, the photogenerated excitons from both donors migrate toward the interfaces and then dissociate into free carriers and are transported via donors and accepter domains (Figure 3d). As a result, the conditions for both models are less problematic when compared to other models, and they are unaffected by alignments of electronic energy levels and the location of the third components. [21,22,47,48].

3. Solar Cell Parameters

Photoelectric conversion and photovoltaic performance are well known of the parameters that outline the efficiency of the solar cell. Therefore, each parameter such as short circuit current density (J_{sc}), open circuit voltage (V_{oc}), fill factor (FF), and power conversion efficiency (PCE) describes the device performance. The device structure, type, and molecular structure of the active layer materials have a crucial impact on the performance of the photovoltaic devices. Hence, solar cells can be modelled via a p-n junction equivalent circuit to comprehend the photogenerated carriers, recombination, and transporting mechanisms.

In general, there are two models that describe the operation of an organic solar cell (OSC) called the single diode model and the two diode model, which are depicted in Figure 4 [49]. The current source in the equivalent circuit represents the junction in which the excitons are dissociated into a free carrier upon harvesting photons and is connected in parallel with a forward diode (D_F) as well as a shunt resistance (R_{sh}). The diode acts as a short circuit in the condition of forward bias, whereas in reverse bias condition, it acts as an open circuit. Consequently, the shunt resistance indicates the recombination processes after the excitons are dissociated near the junction site, and at the reveres bias condition, designates the resistive pass of the leakage current. In addition, a series resistance(R_s) reflects the transport mechanism of free carriers through organic active layer toward the respective electrodes. Hence, it depends on the resistivity of organic materials, electrodes, and organic material/electrode interfaces, which is alternatively influenced by space charge, traps, and hoping. In the single diode model, the current density (J) ascribed by the Shockley equation as shown in Equation 2 [50].

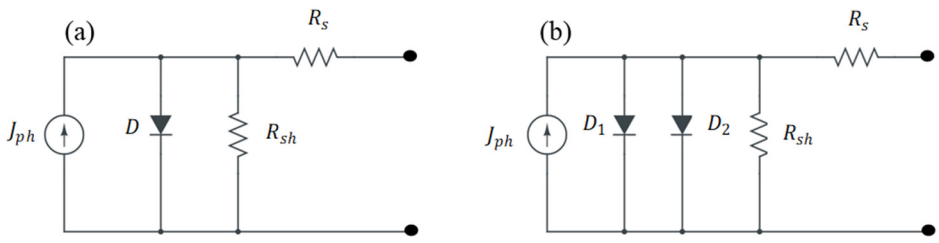

Figure 4. solar cell equivalent circuit for (**a**) single diode model, and (**b**) two diode model (authors created illustration).

Preprints (www.preprints.org) | NOT PEER-REVIEWED | Posted: 10 July 2023 doi:10.20944/preprints202307.0522.v1

$$J = J_{ph} - \frac{V+JR_s}{R_{sh}} - J_0\left[exp^{\left(\frac{q}{\beta kT}[V+JR_s]\right)} - 1\right] \quad (2)$$

Where J_{ph} and J_0 are the photogenerated current density and saturation current density at reverse bias conditions, respectively, $V$is the cell voltage, β is the diode ideality factor, q is the electronic charge, k is the Boltzmann's constant, and T is the temperature. In this model, the ideality factor is equal to 1 and it is a function of the voltage across the cell. However, at low voltage the recombination of free carriers at the junction becomes dominant and the value of β goes to two.

Therefore, by adding the second diode (Figure 4b) the recombination at the junction can be considered and the current density (equation 2) modified under illumination as shown in the following equation:

$$J = J_{ph} - \frac{V+JR_s}{R_{sh}} - J_{01}\left[exp^{\left(\frac{q}{\beta kT}[V+JR_s]\right)}\right] - J_{02}\left[exp^{\left(\frac{q}{\beta kT}[V+JR_s]\right)}\right] \quad (3)$$

The photoactive layer in an organic solar cell possesses low dielectric permittivity and localized properties of electronic state at the optical excited state create a built in potential which hinders the exciton dissociation. Therefore, the photogenerated current density as shown in equation 4 depends on the absorption profile of the active layer and the solar irradiance spectrum (Figure 5) [51,52]

$$J_{ph} = \frac{q}{hc}\int A(\lambda)AM1.5G(\lambda)\lambda d\lambda \quad (4)$$

where h is the Plank's constant, q is the electric charge, $A(\lambda)$ is the spectral response of absorbance of the active layer, c is the speed of light and $AM1.5G(\lambda)$ is the spectral irradiance of the sunlight. Hence, the maximum current stream out into the external load, due to the external field, is called the short circuit current density(J_{sc}). With the assumption that all the photogenerated carriers are collected by the respective electrodes without recombination, the photo generated current density would be equal to the short circuit density [4].

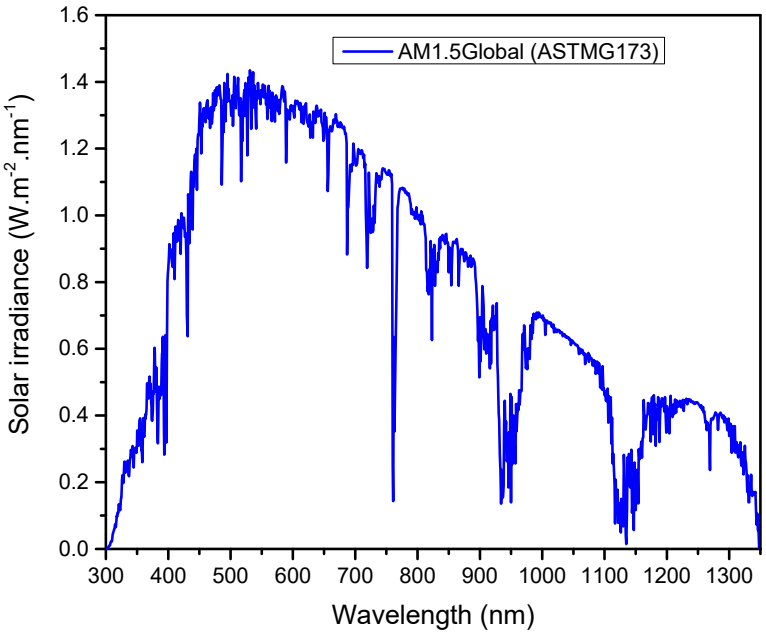

Figure 5. Spectral irradiance of the Sun (AM1.5 Global spectrum) (authors created illustration).

Nevertheless, all photogenerated carriers cannot be migrated toward the respective electrodes due to recombination processes either at the active layer or at the interface of the active layer/electrodes. In addition, at forward bias conditions, the direction of forward current

Preprints (www.preprints.org) | NOT PEER-REVIEWED | Posted: 10 July 2023 doi:10.20944/preprints202307.0522.v1

(recombination current) is opposite to the direction of photogenerated current, and due to the decrease in barrier potential, the forward current increases until it becomes equal to the photogenerated current. As a result, the current density at the external load becomes zero. At this point, the voltage is called the open circuit voltage (V_{oc}) and hence the series resistance can be neglected, whereas the internal voltage equals to the open circuit voltage. Thus, the (V_{oc}) can be determined by solving Equation 2 [25]:

$$\boldsymbol{V_{oc} = \frac{\beta kT}{q} ln\left(\frac{J_{ph}(V_{oc})}{J_0} + 1\right)} \quad (5)$$

Accordingly, the stability between the rate of photogeneration and the rate of recombination determines the V_{oc}. Hence, it extremely depends on the band gap of the active layer. Herein, the voltage loss from the differences between the energy gap of the active layer and the voltage across the cell V_{oc} observed. This is due to the existence of radiative and non-radiative recombination and energy offset at interfaces between donor and acceptor, which are required for charge transfer energy state [53].

Both short circuit current density and open circuit voltage can be obtained experimentally from the $J-V$ characteristics of solar cells, as depicted in Figure 6. In this schematic, both V_m and I_m represent the maximum value of voltage and current delivered to the external load. Thus, by multiplying both of them, the maximum output power can be calculated (equation 6). The additional parameter which designates the relationship between collection and recombination of the free carriers might be extracted from the $J-V$ characteristics of the solar cell (see equation 7) and it is called the fill factor (FF). Therefore, the power conversion efficiency (PCE) of the solar cell can be measured by dividing the maximum output power P_m of the cell into the incident light input powerP_{in}, as stated in Equation 8 [7,54].

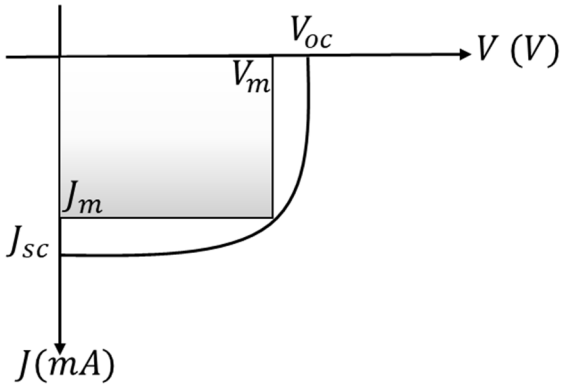

Figure 6. Schematic of typical $J-V$ characteristics of solar cell under illumination.

$$\boldsymbol{P_m = V_m \times J_m} \quad (6)$$

$$\boldsymbol{FF = \frac{V_m \times J_m}{V_{oc} \times J_{sc}}} \quad (7)$$

$$\boldsymbol{\eta = \frac{P_m}{P_{in}} \times 100\% = \frac{FF \times V_{oc} \times J_{sc}}{P_{in}} \times 100\%} \quad (8)$$

As previously stated, the charge transport mechanisms in a ternary system are more complex than those in a binary system due to the addition of the third component. Therefore, the third component has a crucial role in defining the solar cell efficiency as well as the device parameters. To this end, the absorption spectra of the third component should remain complimentary to the spectrum of the host binary system, hence a substantial improvement is observed for short circuit current density (J_{sc}) (see Equation 4). Therefore, for each transport model, the J_{sc} improves considerably while the V_{oc} experiences a non-monotonic variation. This is because V_{oc} depends on quasi-Fermi levels of the absorber layer. Alternatively, the addition of the third component affects

Preprints (www.preprints.org) | NOT PEER-REVIEWED | Posted: 10 July 2023 doi:10.20944/preprints202307.0522.v1

the degree of crystallinity and phase separation, leading to different types of traps and recombination, which consequently all parameters are subjected to considerable variations. Thus, identifying the loss mechanism and careful designing of the ternary system required for high efficiency and stable solar cell [19,22]. Therefore, recombination processes are categorized into two types: geminate and non-geminate recombination. At geminate recombination the electron-hole pairs recombine before dissociation or at charge transfer state (CT) while at non-geminate recombination, free electrons and free holes are considered once the free charges drifted toward the electrodes and it is classified into bimolecular, trap-assist, and Auger recombination.

It is worth mentioning that there are numerous factors influencing the recombination processes, the charge extraction process and device performance. For example, the mobility of charge carriers, film thickness of the active layer, phase separation, impurity, and energetic disorder have emerged to be parameters that are involved in non-geminate recombination. The energy offset at the interface, domain size, molecular rearrangement, phase purity, internal electric field, and delocalized charge transfer state all influence the rate of geminate recombination or excitons dissociation [55]. Meanwhile, tremendous efforts have been made and led to the improvement of the performance of the ternary organic solar cells. Tuning the optical band gap of the active layer inspired the careful fabrication of semi-transparent organic solar cells using various materials ranging from high to low band gap. Consequently, the photon harvesting in the ultraviolet and near infrared regions and the thickness of the active layer can be enhanced by selecting suitable organic materials. Additionally, the difference between opaque and semi-transparent organic solar cells is that the cell is transmitted at a visible range.

Consequently, all the parameters which evaluate the opaque device performance can be used for semi-transparent alongside with several other parameters such as average visible transmittance (AVT), colour properties, quantum utilization efficiency (QUE) and light utilization efficiency (LUE). AVT is a measure of transparency of the cell in the range of $(370nm - 740nm)$ with respect to the photonic response to human eye and it can be determined from Equation (9). In the window application, the reference value of (AVT) considered to be 25% [33].

$$\boldsymbol{AVT} = \frac{\int \boldsymbol{T(\lambda)} \times \boldsymbol{V(\lambda)} \times \boldsymbol{AM1.5G(\lambda)d\lambda}}{\int \boldsymbol{V(\lambda)AM1.5G(\lambda)d\lambda}} \tag{9}$$

Where $V(\lambda)$ is the photonic response of the human eye, $T(\lambda)$ is the transmission spectrum of the device, and $AM1.5G(\lambda)$ is photon flux under AM 1.5G light illumination. Moreover, for practical applications, the color properties of the device play a critical role in the visual appearance perceived by the human eye and the perception of colour transparency first measured by Ameri et al. using the CIE 1931 xyz chromaticity diagram. In semi-transparent OSCs, the quantitative parameter that shows the degree of colour rendering between illuminations and transmissions of light through the device is called colour rendering index (CRI) and can be estimated by comparing the natural source of light to the test light source [56]. In addition to the ability of the ST-OSCs of photon harvesting, its conversion and visibility, a set of impartial parameters can be utilized for device performance. The first one is called quantum utilization efficiency (QUE), which is defined by the summation of external quantum efficiency (EQE) and transmittance (T) of the cell (equation 10). Thus, the value of QUE should be less than 90% over visible region due to essential intrinsic losses. The second metric, which is crucial to calculate the performance of the cell and best uses of light, is light utilization efficiency (LUE). This can be measured through multiplying the power conversion efficiency (PCE) by the average visible transmittance (AVT), as shown in Equation (11) [36].

$$\boldsymbol{LUE} = \boldsymbol{PCE} \times \boldsymbol{AVT} \tag{10}$$

$$\boldsymbol{QUE} = \boldsymbol{EQE} + \boldsymbol{T} \tag{11}$$

Preprints (www.preprints.org) | NOT PEER-REVIEWED | Posted: 10 July 2023 doi:10.20944/preprints202307.0522.v1

4. Photoactive Layer Characterization

Due to promising applications in semitransparent photovoltaic devices, polymer solar cells are strongly contributing to the production of future large area and cost-effective devices. Therefore, a broad study of the photoactive layer is essential for better assessment of the photogeneration of excitons and their separation at the interface between donor and acceptor materials, along with the transport mechanism toward the respective electrodes. Hence, photophysical, electrochemical, and spectroscopic characteristics are required to broadly examine the photoactive layer, including energy gap, electronic energy levels (HOMO and LUMO), type of functional groups, and optical constants.

4.1. Photophysical Characterization

To evaluate the photophysical properties of the photoactive layer, UV-Vis absorption spectroscopy can be used. It is well known from literature that the absorption bands in the UV region can be ascribed to the $\pi - \pi^*$ and $n - \pi^*$ transitions of delocalized excitons in the polymer chain, whereas the absorption bands in the visible range are assigned to intramolecular charge transfer (ICT) between electron-rich moiety and electron-deficient moiety of the main chain [57,58]. Hence, the absorption coefficient (α) can be determined from the absorbance data by using Equation 12 as well as the optical constants can be estimated using Equations 13 to 21 [59].

$$\alpha = \frac{2.303A}{t} \tag{12}$$

$$n = \frac{-2(R+1) \pm \sqrt{4k^2R^2 + 16R - 4k^2}}{2(R-1)} \tag{13}$$

$$k = \frac{\alpha\lambda}{4\pi} \tag{14}$$

Where t is the thickness of photoactive layer, A is the absorbance and R is the reflectance and can be calculated by using the following equation: $R = 1 - T - A$, where T is transmittance and estimated from $T = 10^{-A}$. Consequently, prior to device manufacturing, the optical constants such as refractive index (n) and extinction coefficient (k) and their derivative parameters like dielectric constant (ε) and optical conductivity(σ) should be considered.

By studying the refractive index of the photoactive layer, it is possible to reveal how the electromagnetic wave spreads throughout the photoactive materials and the change of the speed inside the material with respect to the vacuum. Moreover, it is a complex variable, and the imaginary part indicates the amount of energy lost due to the medium, which is called extinction coefficient. Additionally, optical dielectric constant (ε) is a frequency dependent parameter and shows the electron response to the incident photon in the material, while the dissipation factor ($\tan\delta$) attributes to the rate of absorption. Meanwhile, the dielectric constant is a complex function, and its real part is assigned to polarization upon the impact of electromagnetic field, whereas the imaginary part illustrates the optical loss and can be described by the following equations:

$$\varepsilon = \varepsilon_1 + i\varepsilon_2 \tag{15}$$

$$\varepsilon_1 = n^2 - k^2 \tag{16}$$

$$\varepsilon_2 = 2nk \tag{17}$$

$$\tan\delta = \frac{\varepsilon_2}{\varepsilon_1} \tag{18}$$

Where $\varepsilon_1$represents the real part and ε_2 represents the imaginary part of dielectric constant. The crucial parameter, which can be used to refer to the electron response to the absorbed photon, is optical conductivity. Since the optical conductivity is derived from the optical dielectric constant, it is a complex variable, and the following equations define both parts of the optical conductivity:

Preprints (www.preprints.org) | NOT PEER-REVIEWED | Posted: 10 July 2023 doi:10.20944/preprints202307.0522.v1

$$\sigma^* = \sigma_r + i\sigma_i \tag{19}$$

$$\sigma_r = \omega\varepsilon_2\varepsilon_o \tag{20}$$

$$\sigma_i = \omega\varepsilon_1\varepsilon_o \tag{21}$$

Where ω is the angular frequency, $\varepsilon_o$is the permittivity of free space, σ_r and σ_i are the real and imaginary part of complex optical conductivity, respectively.

4.2. Energy gaps and transition types

In ternary systems for photovoltaic devices, it is imperative to identify the transport mechanism from the alignment of electronic energy levels and the value of the energy gap. Hence, it is possible to measure the optical energy gap and the type of optical transitions of the photoactive layer from absorption spectra by using Tauc's equation or from the absorption edge of the absorption spectrum as follows [60,61]:

$$\alpha h\nu = \alpha_o(h\nu - E_g)^s \tag{22}$$

$$E_g = \frac{1242}{\lambda_{onset}} \tag{23}$$

However, Tauc's equations can be assigned directly to ascribe the nature of transition despite the measuring of the optical energy gap, by taking the natural logarithm and derivation of Equation 22 [62],

$$\frac{d\,ln(\alpha h\nu)}{d(h\nu)} = \frac{s}{h\nu - E_g} \tag{24}$$

Where E_g is the energy gap, $\alpha_o$is an energy-independent constant, and the value of s defines the type and nature of transitions[63]. If the value of $s = 2$, the transition is indirect allowed transition and $s = 3$ is for indirect forbidden transitions, $s = \frac{1}{2}$ for direct allowed transition , $\frac{3}{2}$ for direct forbidden transitions. Meanwhile, to estimate the electronic energy levels, the electrochemical study provides comprehensive information regarding the position of HOMO and LOMO levels of organic materials prior to device fabrication. Cyclic voltammetry (CV) is the most accurate method used to estimate energy levels from oxidation and reduction potentials. The oxidation and reduction potentials are selected from the onset potential, which is defined as the potential where holes or electrons initially injected to HOMO and LUMO levels, respectively, and hence the rise of anodic or cathodic current become obvious. To estimate E_{LUMO}, E_{HOMO} and $E_g^{CV}$the relation below is used with Ferrocence as the reference electrode [64]:

$$\boldsymbol{E_{HOMO} = -\left(E_{(onset,ox\ vs.Fc^+/Fc)} + 5.39\right)(eV)} \tag{25}$$

$$\boldsymbol{E_{LUMO} = -\left(E_{(onset,red\ vs.Fc^+/Fc)} + 5.39\right)(eV)} \tag{26}$$

$$\boldsymbol{E_g^{CV} = E_{HOMO} - E_{LUMO}} \tag{27}$$

The estimated gap from HOMO to LUMO level, which is found from the CV measurement, is defined as a minimum energy formation of a detached and connected with the transport of a single particle. The optical energy gap corresponding to the formation of an exciton and interestingly has a larger value due to the binding energy of excitons.

5. Materials for Semi-Transparent Organic Photoactive Layer

Since the discovery of π-conjugated polymers in the early nineteenth century, the focus of renewable energy research has switched to the design and application of π-conjugated polymers. In comparison to their inorganic semiconductor counterparts, the π-comjugated polymers possess a

variety of advantages such as solution processability, flexibility, and electrical and optical tunability via structural modifications. Alternatively, the side chains of the polymeric backbones improve their properties, which permits them to assemble nanostructured layers easily. Also, due to the rich nature of π bonds of the conjugated polymer backbones, accepter and donor units can be produced. Hence, the energy gap and electronic energy level of these materials demonstrate tunability and intramolecular charge transfer. To some extent, conjugated polymers have found several uses in different types of photovoltaic applications, including donor and accepter materials as well as hole and electron transport layers [65].

In organic solar cells, several architectures evolved from bilayer heterojunction to bulk heterojunction structures of donor and accepter organic semiconductor materials. Because of the low dielectric constant and low diffusion length of excitons, the research trends of the bulk heterojunction (BHJ) structure become dominant and exhibit considerable efficiency. In this class of photovoltaic devices, the donor and acceptor materials are mixed at solution phase and form a single junction binary heterojunction structure. Thus, the interface layer increases, and the thickness of the active layer can be reduced to around 100 nm which is favourable for exciton diffusions and dissociations.

The conventional organic materials were used are Poly(3-hexylthiophene-2,5-diyl) (P3HT), and the fullerene, in particular [6,6]-Phenyl-C61-butyric acid methyl ester (PCBM) as a donor and acceptor materials, respectively, which they showed a limited efficiency and stability. Despite fullerenes' frequent use due to high electron mobility, isotropic charge transport, good electron affinity, and good compatibility, whereas the increases of PCE were limited because of weak absorption in the near infrared region NIR, the limitation of energy level tunability, as well as the migration and aggregation of fullerene nanoparticles in the solid phase. Therefore, numerous non-fullerene acceptors were synthesised along with synthesises of a variety of donor materials for enhancing device performance [34,66].

Furthermore, in semi-transparent organic solar cell (ST-OSC) a trade-off is present between transparency and photon harvesting in the visible region. Therefore, the thickness and the type of materials in the active layer show a considerable effect on the device performance. As such, synthesis of new polymers/small molecules or the addition of the third component to the photoactive layer are the alternative approaches toward enhancing both transparency and device performance. Semi-transparent ternary systems are generally composed of two donors and an acceptor or a donor and two acceptors, so the materials used are all polymers or polymers with small molecules or dyes. Based on the solar irradiance spectrum (Figure 5) the UV and NIR regions account for about 2% and 51% of the solar power, respectively, whereas the visible region accounts for about 47%. Therefore, in the design of an active layer with high performance, there should be a strong photon absorption in the UV, NIR, and IR regions and high visibility in the visible region. For that reason, the energy gap of the raw materials plays an important role for photon harvesting and charge collection. So the conventional classification for organic solar cells is based on fullerene and non-fullerene solar cell [36].

Poly(3-hexylthiophene) (P3HT) is the conventional donor material that was used in photovoltaic devices because at solid phase it has a strong tendency of self-assembling into crystal phases. However, P3HT cannot be a prominent candidate for the ST-OSC due to strong absorption in the visible region and poor hole mobility, which limit the thickness of the absorbing layer [67]. For example, Çetinkaya et al. fabricated a binary semi-transparent solar cell with the structure of (FTO/ZnO/P3HT:PCBM/MoO3/Ag/MoO3), in which they observed that the average visibility (AVT) is about 37%, whereas the efficiency of the device was around 1.77% [68]. In addition, Bliznyuk and co-workers introduced an organic dye into a P3HT:PCBM binary system and extend the absorption spectrum to near the IR region and transparent in the visible region; however, the efficiency of the ternary systems was in the range of (0.04 -0.4)% for different compositions and efficiency was decreased compared to that of the standard binary system due to the reduction in the thickness of the active layer and traps that where introduced upon inserting the low energy gap materials [69].

Nonetheless, Xie et al. fabricated (ITO/ PEDOT:PSS/PTB7-Th:PBT1-S:PC71BM/MoO3/Ag) fullerene based ST-TOSC and the conventional donor replaced by PTB7-Th with inserting a high band

Preprints (www.preprints.org) | NOT PEER-REVIEWED | Posted: 10 July 2023 doi:10.20944/preprints202307.0522.v1

gap ($E_g = 2.1\ eV$) PTB1-S polymer as a second donor with different weight ratios. Therefore, the optimized efficiency (10.3%) of the opaque ternary device was observed at 10wt% of the third component while the trade-off between AVT and PCE for the semi-transparent device was observed. The optimized AVT for the ternary system has been achieved by reducing the thickness of the top electrode, but the PCE was reduced to its minimum value. For example, the device with 5 nm Ag thickness experienced 44.8% of average visibility and 5% of device efficiency [70]. Very recently, Liu and co-workers designed a new low band gap non-fullerene acceptor for ST-TOSCs and the enhanced device performance for the active layer consisted of PM6: SN: Y6 (D: A1:A2). For this device, a PCE of 14.0 % at an AVT of 20.2% was reported [71].

Additionally, nanomorphology of the active layer is another key parameter that determine the device efficiency. In BHJ structure, the low mixing entropy and the entanglement of the polymer chain directly affect the domain size and phase separation. Hence, both molecular stacking and its orientation followed by the crystallization and aggregation of the materials define the charge transfer efficiency [72]. For instance, Heng and co-researchers prepared a ternary system consisting of PTFBDT-BZS:ITIC with the fullerene as the third component. This study shows that by increasing the weight ratio of $PC_{71}BM$ up to 40% the domain size of ITIC was reduced and phase separation was improved. Furthermore, this study suggests that with larger amount of the third component inhibited the large aggregation and hence reduced the domain size [73]. In addition, Liu and co-researcher investigated the effect of domain size on the device performance. In their study, the binary system of PBDB-T/N2200 treated thermodynamically in solution state, thereby obtaining a film with a proper domain size and preserved degree of crystallinity [74].

5.1. Dye Materials for Semitransparent Solar Cells

Small molecule dyes have become the focus of interest in both industry and academia due to the unique features offered by the dye molecules, including electronic tuneability, flexibility, cost-effectiveness, and light weight properties. Moreover, organic dyes show a higher absorption coefficient and stronger exciton generation compared to those of inorganic materials. Synthesized dyes are commonly used in various applications, especially photovoltaic applications. For instance, several synthesized dyes such as cyanine dye, squaraine dye, Azo dye and its derivatives have been employed in different structures of polymer photovoltaic devices, including semi-transparent and opaque structures [75–79]. Makha et al. fabricated an inverted semitransparent ternary OSCs with an AVT of 51% and a PCE of 3% by incorporating a small molecule of Cyanine dye (Cy7-T) into a host binary system of PBDTTT-C: $PC_{70}BM$[78]. Nevertheless, these synthesized dyes suffer from high cost, supply shortage, heavy metal toxicity, and challenging synthesis, which ultimately limit their broad usage.

Alternatively, the appealing natural dyes can overcome these limitations such as Carotene, Chlorophyll, Anthocyanin and betalain dyes with their derivatives which show a prominent candidate as one of the components of the active medium materials for light harvesting in ternary ST-OSCs. For instance, Vohra and co-workers employed a natural dye as an electron donor named β-carotene (bCar) and blended it with a fullerene acceptor to form the BHJ structure. As a result, the inverted structure of the organic solar cell experienced a fill factor of around 35% and its efficiency was about 0.58% [80]. Moreover, Duan et al. studied the aggregate Chlorophyll as a p-type organic semiconductor in both bilayer and BHJ structures and used it with the fullerene acceptor. The device performance showed the power conversion efficiencies around 5% and 3.5% for both BL and BHJ structures, respectively [81]. Furthermore, these natural dyes were used in all organic-based devices such as Perovskite solar cells, dye sensitised solar cells (DSSCs), and organic light emitting diodes (OLEDs), but no reports focused on using these dyes in semi-transparent ternary organic solar cells.[82–84].

5.2. Non-Fullerene Acceptors

Because of its noble electron transport capabilities, fullerene acceptors and their derivatives were employed in the BHJ structure, which is now the standard structural design for the manufacturing of

Preprints (www.preprints.org) | NOT PEER-REVIEWED | Posted: 10 July 2023 doi:10.20944/preprints202307.0522.v1

organic solar cells. These fullerene-based materials, on the other hand, exhibit low optical absorption and limited energy level tunability. As the donor component is responsible for optical absorption, the tiny absorption window that the respective device possesses hinders the device's efficiency.

Therefore, several approaches have been made to broaden the absorption window, which leads to enhanced photocurrent density, consequently device efficiency as well as photochemical stability. Alternatively, designing a new n-type organic semiconductor named non-fullerene acceptor draws extensive attention. This is because the non-fullerene acceptor can be synthesised in a facile process, also preserves the good electron mobility compared to it fullerene counterparts and shows outstanding photochemical stability. Interestingly, the energy gap of these organic semiconductors can be tuned and therefore the absorption window can be modified. Furthermore, several families of non-fullerene acceptors were synthesised and employed in photovoltaic applications, showing promising outcomes [25,40,85,86].

Recently, the non-fullerene acceptors have been widely employed in both opaque and semi-transparent ternary BHJ organic solar cells and the respected devices exhibited a high performance. For instance, Wang et al. fabricated both ternary opaque and semi-transparent devices, which consist of PM6:Y6:IT-M, and due to balanced charge transport and smooth morphology of the ternary system, the photocurrent density was improved. The PCE for the opaque ternary device was around 15% and the PCE and AVT for the semitransparent ternary device was around 11% and 22%, respectively [87]. Additionally, Liu and co-workers employed a non-fullerene acceptor IEICO-4F as a host acceptor blended with PTB7-Th as a donor. By combining 20 wt% of NCBDT-4Cl, the ternary system was formed and the optimum PCE and AVT of ternary ST-PSCs were recorded to be 10.31% and 20.6%, respectively [88]. Table 1 shows the recent developments in the materials including fullerene and non-fullerene acceptor and third components for semi-transparent ternary system.

Table 1. Summary of materials progress used in ST-OSCs.

Reference	Donor Materials	Acceptor Materials	Third Components	Device Efficiency	
				PCE (%)	AVT (%)
[89]	PTB7-Th	PC71BM	PBT1-S	9.2	20
[90]	PM6	Y6	IHIC (20%)	12.18	27.07
[71]	PM6	Y6	SN	14	20.2
[91]	PBDB-TF	Y6	BDC-4F-C8	13.19	24.56
[92]	PM6	Y6	DIBC	14	21.6
[93]	PTB7-Th	BDTThIT-4F	IEICO-4F	9.4	24.6
[94]	PM2	Y6-BO	-	7.9	-
[88]	PTB7-Th	IEICO-4F	NCBDT-4Cl	10.31	20.6
[95]	PBDB-TF	Y6	DTNIF	13.49	22.58
[96]	D18-Cl	Y6	Y6-1O	13.02	20.2
[97]	PBDB-T	Y1	PTAA	12.1	20.1
[98]	J71	IHIC	PTB7-Th	9.37	21.4
[98]	PBDB-T	IHIC	PTB7-Th	8.76	20.6

6. Approaches to Improve Semi-Transparent OSCs

6.1. Active Layer Strategies

As previously stated, the primary distinction between opaque and semi-transparent organic solar cells is their visible region transparency. Hence, to achieve this condition, several approaches have been proposed by the researchers, as shown in Figure 7 and Table 1. For instance, Hu et al. and Cheng et al. utilized large band gap polymers to obtain semi-transparent solar cells. The broad bandgap polymer D18-Cl (HOMO:-5.48 eV/ LUMO:-2.75 eV), narrow bandgap material Y6-1O (HOMO:-5.71 eV/ LUMO:-3.84 eV) and the narrower bandgap material Y6 (HOMO:-5.65 eV/ LUMO:-4.10 eV) were used by Hu and co-workers as an active layer of the semi-transparent OSCs. Two

 doi:10.20944/preprints202307.0522.v1

approaches were utilized to convert the opaque cell into semi-transparent cell. First, by adjusting the weight ratio of donor and acceptor, and second by reducing the thickness of the top electrode [96]. Moreover, Cheng and co-workers employed a large-bandgap polymer (poly[bis(4-phenyl)(2,4,6-trimethylphenyl) amine (PTAA)) as partial substitutions for the donor material and as a hole transport layer of the ST-OPVs. Thus, the inclusion of PTAA into a binary system has led to enhance the visibility of the device in the visible region and improve the film morphology [97].

In addition, reducing the thickness of the active layer is another approach for converting opaque structure to semi-transparent structure. For instance, Lu et al. utilized a small molecule of DIBC as a third component into a binary PM6:Y6 host system. The stability and thickness tolerance of active layer were demonstrated, and it was found that due to hydrogen intermolecular bonds, the aggregation of photo sensitive materials can be enhanced. Therefore, extra channels for charge transport are facilitated because of the presence of more contact interfaces. Consequently, incorporation of a small portion of the hydrogen bond via inserting DIBC hinders both bimolecular recombination and trap-assisted recombination [92].

On the other hand, the weight ratio adjustment of the components of the photoactive layer was used for enhancing semi-transparent solar cells. Hu and co-workers employed a narrow band gap material as a host binary material and investigated the effect of weight ratio of the third component. In addition, IEICO-4f as an ultra-narrow gap form an alloy with the host acceptor material due similar electronic energy (HOMO and LUMO) levels [93], and the optimum weight ratio was found to be 50%. Moreover, Wang et al. balanced the trade-off between PCE and AVT upon inserting (10%wt) of BTTPC acceptor into the host binary blend. Because of the enhancement of the rate of hole transport, the charge recombination was reduced in the ternary blend. Also, further improvement was observed for AVT without affecting the PCE due to the application of photonic reflector [99].

Non-fullerene acceptors with narrow band gap were broadly used for semi-transparent applications. For instance, Yin and co-workers utilized a non-fullerene acceptor (DTNIF) to enhance both V_{oc} and to balance the charge transport when 10% of weight ratio added into the host materials. The improvements were achieved because the DTNIF has a high LUMO energy level compared to that of the acceptor Y6 and the increase of the crystallinity phase in the ternary blend with decreasing the distance of π-π stacking [95].

Moreover, blending fullerene acceptor with non-fullerene acceptor has led to establish a long-term stability and enhance the film morphology. For example, Sano et al. demonstrated that by adding a non-fullerene acceptor (ITIC) into the binary active layer (PCDTBT:PC71BM) the devices exhibited a long-term operational stability. Furthermore, PC71BM, with ITIC yielded a uniform absorption spectra [38]. Remarkably, absorption spectra for the ternary system were used as an experimental tool to find the optimal weight ratio, at which the device shows a maximum photocurrent. In addition, the third component (BDC-4F-C8) was used as a crystallization agent to enhance the crystallinity of the binary system [100]. Meanwhile, small molecule dyes and wide band gap polymers might have the potential for semi-transparent photovoltaic cells due to the ability of these materials to extend and continuous the absorption spectrum in both directions (blue shift or red shift). For example, Tang et al. proposed a wavelength selective semi-transparent OSCs bulk heterojunction structure by blending a wide bandgap small molecule TAPC $\left(E_g = 3.54\ eV\right)$ with a non-fullerene Y6 and the optimized parameters for ST-OSCs attained an overall PCE of 3.01% with a high AVT of 47.99% [101].

Preprints (www.preprints.org) | NOT PEER-REVIEWED | Posted: 10 July 2023 doi:10.20944/preprints202307.0522.v1

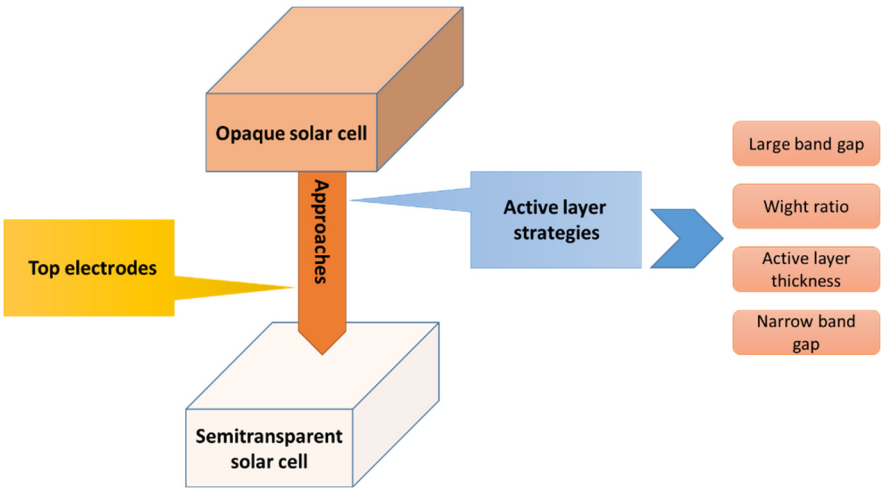

Figure 7. Illustration of approaches for converting opaque to semitransparent solar cells (authors created illustration).

6.2. Transparent Top Electrodes

For achieving highly efficient semitransparent OSCs, high transmittance in the visible region, reflectance in both UV and IR regions, and high conductivity for both electrodes are prerequisites, whereas the compromise between high transmittance and high conductivity of the top electrode is prevalent. Thus, device engineering and selection of electrode materials are very crucial for device operation. To date, several types of top electrodes have been employed in photovoltaic devices, as shown in Figure 7. However, each type of top electrode shows strength and weakness.

As shown in section 5, most recent studies utilize thin metal layers as a top electrode. Nevertheless, a tradeoff is observed between AVT and PCE, which is employed by decreasing the thickness of the top electrode. Consequently, the visibility increases while the efficiency decreases. Alternatively, metal nanowires such as Ag nanowires have the potential to overcome the compromise between conductivity and transparency of top electrodes. Flexibility and solution processability along with interesting optoelectronic properties measured as the strength of Ag nanowires, whereas poor adhesion, roughness, and device stability are considered drawbacks and hinder the improvement of the device performance. Therefore, several studies contribute to improve Ag nanowires [78,102–104] and recently Sannicolo et al. used Ag nanowires as a back electrode and stabilized with graphene oxide sandwich layers. Concludingly, the graphene oxide layer serves to encapsulate the hole transport layer and optimize its adhesion to the top electrode, as well as protect the top electrode from the acidity of PEDOT:PSS interface layer [105].

Another type of transparent top electrode is conductive oxides such as indium tin oxide (ITO) and Al-doped zinc oxide (AZO) that possess excellent optoelectronic properties. Generally, ITO is used as the bottom electrode and due to its high conductivity and transparency, it can also be used as a top electrode. However, due the deposition process, which can be done by magnetron sputtering, the photo absorber layer might be damaged which results in a poor device performance [106]. Therefore, Huang et al. proposed a laminated technique for assembling ITO as a top electrode, where the modified PEDOT:PSS was used as an adhesive layer for assembling the device [107].

Preprints (www.preprints.org) | NOT PEER-REVIEWED | Posted: 10 July 2023 doi:10.20944/preprints202307.0522.v1

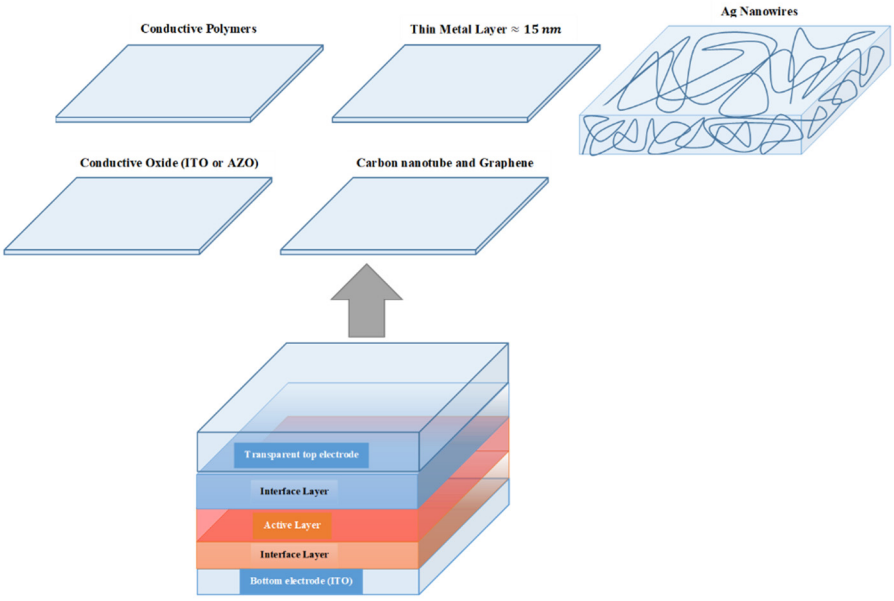

Figure 7. Illustration of different types of semitransparent top electrodes (authors created illustration).

For flexible semitransparent organic solar cells, carbon nanotubes and graphene are favorable for transparent top electrodes due to high transparency in the visible region, chemical stability and mechanical flexibility. However, a survey from literature showed that the device efficiency is around (1-4) %, which is due to the low conductivity of the top electrodes but exhibits good stability and long lifetime [33,34]. Furthermore, the promising candidate of transparent top electrodes for all solution processability of semitransparent OSCs is poly (3,4-ethylenedioythiophene)-poly-(styrenesulfonate)(PEDOT:PSS;PH1000), which exhibits a high transparency in the visible range, low temperature solution processability, and tunable conductivity.

7. Conclusions

One of the endeavors to increase power conversion efficiency (PCE) while conserving flexibility, easy fabrication and low cost is the ternary system for bulk heterojunction active layer. The ternary system improves light harvesting by broadening the spectral response of the active layer. A ternary system comprises a combination of three components, including donor, acceptor, and third components. Therefore, selecting the third component is a remarkable consideration for device performance. The materials used in the BHJ structure were categorized based on their structures, including polymers, small molecules, nanostructures, and dyes. Hence, selecting the third component in a ternary system induces more convolution in the charge transport mechanism, whereas it can enhance the absorption profile, exciton dissociation, charge transport, and film morphology. Moreover, the ability of organic materials to tune their bandgap energy revealed a new field of practices entitled semi-transparent organic photovoltaics (ST-OPV). Additionally, in semi-transparent organic solar cell (ST-OSC) a trade-off is presented between transparency and photon harvesting in the visible region; therefore, the thickness and the type of materials in the active layer show a considerable effect on the device performance. Consequently, synthesis of new polymers/small molecules or the addition of the third component into the photoactive layer are the alternative approaches toward enhancing both transparency and device performance. Despite this progress, more research on photoactive materials is needed to fully understand the working mechanisms of ternary systems as well as device stability.

Author Contributions: POA: Writing - original draft preparation; FFM, SRS, KAK: Writing-review and editing.

Funding: "Funding is not available for this work"

Institutional Review Board Statement: "Not applicable" for studies not involving humans or animals.

Data Availability Statement: The data and material are available within the manuscript.

Acknowledgments: The authors gratefully acknowledge the Ministry of Higher Education and Scientific Research-Kurdistan Regional Government-Charmo University—College of Medical and Applied Science — Department of Medical Physics for the financial support.

Conflicts of Interest: The authors declare that there is no conflict of interest regarding the publication of this paper.

References

1. Tsai, C.-H.; Lin, C.-M.; Kuei, C.-H. Investigation of the Effects of Various Organic Solvents on the PCBM Electron Transport Layer of Perovskite Solar Cells. *Coatings* **2020**, *10*, 237.
2. Goetzberger, A.; Hebling, C.; Schock, H.-W. Photovoltaic materials, history, status and outlook. *Materials Science and Engineering: R: Reports* **2003**, *40*, 1-46, doi:https://doi.org/10.1016/S0927-796X(02)00092-X.
3. Askari, M.; Mirzaei Mahmoud Abadi, V.; Mirhabibi, M. Types of Solar Cells and Application. *American Journal of Optics and Photonics* **2015**, *3*, 2015, doi:10.11648/j.ajop.20150305.17.
4. Andreani, L.C.; Bozzola, A.; Kowalczewski, P.; Liscidini, M.; Redorici, L. Silicon solar cells: toward the efficiency limits. *Advances in Physics: X* **2019**, *4*, 1548305, doi:10.1080/23746149.2018.1548305.
5. Bhattacharya, S.; John, S. Beyond 30% Conversion Efficiency in Silicon Solar Cells: A Numerical Demonstration. *Scientific Reports* **2019**, *9*, 12482, doi:10.1038/s41598-019-48981-w.
6. Lee, C.; Lee, S.; Kim, G.U.; Lee, W.; Kim, B.J. Recent Advances, Design Guidelines, and Prospects of All-Polymer Solar Cells. *Chem Rev* **2019**, *119*, 8028-8086, doi:10.1021/acs.chemrev.9b00044.
7. Wang, G.; Melkonyan, F.S.; Facchetti, A.; Marks, T.J. All-Polymer Solar Cells: Recent Progress, Challenges, and Prospects. *Angewandte Chemie International Edition* **2019**, *58*, 4129-4142, doi:https://doi.org/10.1002/anie.201808976.
8. Guguloth, L.; Singh, K.; Reddy Channu, V.S.; Kumari, K. Improved performance of ternary blend polymer solar cells via work function tuning and suppressed interface recombination using hybrid PEDOT:PSS-graphene oxide hole transport layer. *Applied Surface Science* **2021**, *540*, 148266, doi:https://doi.org/10.1016/j.apsusc.2020.148266.
9. Chang, M.; Meng, L.; Wang, Y.; Ke, X.; Yi, Y.-Q.-Q.; Zheng, N.; Zheng, W.; Xie, Z.; Zhang, M.; Yi, Y.; et al. Achieving an Efficient and Stable Morphology in Organic Solar Cells Via Fine-Tuning the Side Chains of Small-Molecule Acceptors. *Chemistry of Materials* **2020**, *32*, 2593-2604, doi:10.1021/acs.chemmater.0c00097.
10. Lin, Y.; Firdaus, Y.; Nugraha, M.I.; Liu, F.; Karuthedath, S.; Emwas, A.-H.; Zhang, W.; Seitkhan, A.; Neophytou, M.; Faber, H.; et al. 17.1% Efficient Single-Junction Organic Solar Cells Enabled by n-Type Doping of the Bulk-Heterojunction. *Advanced Science* **2020**, *7*, 1903419, doi:https://doi.org/10.1002/advs.201903419.
11. Liu, Z.; Wang, N. Efficient ternary all small molecule organic photovoltaics with NC70BA as third component materials. *Dyes and Pigments* **2021**, *187*, 109111, doi:https://doi.org/10.1016/j.dyepig.2020.109111.
12. Khlyabich, P.P.; Rudenko, A.E.; Thompson, B.C.; Loo, Y.-L. Structural Origins for Tunable Open-Circuit Voltage in Ternary-Blend Organic Solar Cells. *Advanced Functional Materials* **2015**, *25*, 5557-5563, doi:https://doi.org/10.1002/adfm.201502287.
13. Chen, W.; Jiang, H.; Huang, G.; Zhang, J.; Cai, M.; Wan, X.; Yang, R. High-Efficiency Ternary Polymer Solar Cells Based on Intense FRET Energy Transfer Process. *Solar RRL* **2018**, *2*, 1800101.
14. Fan, B.; Zhong, W.; Jiang, X.-F.; Yin, Q.; Ying, L.; Huang, F.; Cao, Y. Improved Performance of Ternary Polymer Solar Cells Based on A Nonfullerene Electron Cascade Acceptor. *Advanced Energy Materials* **2017**, *7*, 1602127, doi:https://doi.org/10.1002/aenm.201602127.
15. Sun, C.; Xia, R.; Shi, H.; Yao, H.; Liu, X.; Hou, J.; Huang, F.; Yip, H.-L.; Cao, Y. Heat-insulating multifunctional semitransparent polymer solar cells. *Joule* **2018**, *2*, 1816-1826.
16. Wang, D.; Liu, H.; Li, Y.; Zhou, G.; Zhan, L.; Zhu, H.; Lu, X.; Chen, H.; Li, C.-Z. High-performance and eco-friendly semitransparent organic solar cells for greenhouse applications. *Joule* **2021**, *5*, 945-957.
17. Li, Y.; Huang, X.; Sheriff, H.K.M.; Forrest, S.R. Semitransparent organic photovoltaics for building-integrated photovoltaic applications. *Nature Reviews Materials* **2023**, *8*, 186-201, doi:10.1038/s41578-022-00514-0.
18. Zhao, N.; Zhen, T.; Wu, Y.; Wei, B.; Liao, Y.; Liu, Y. Efficient Semitransparent Organic Solar Cells Enabled by Ag Grid Electrodes and Optical Coupling Layers. *Nanomaterials* **2023**, *13*, 1308.
19. Adil, M.A.; Iqbal, M.J.; Zhang, J.; Wei, Z. Unconventional third components for ternary organic solar cells. *Materials Today Energy* **2021**, *21*, 100728, doi:https://doi.org/10.1016/j.mtener.2021.100728.
20. Yu, R.; Yao, H.; Hou, J. Recent progress in ternary organic solar cells based on nonfullerene acceptors. *Advanced Energy Materials* **2018**, *8*, 1702814.
21. Ameri, T.; Khoram, P.; Min, J.; Brabec, C.J. Organic ternary solar cells: a review. *Advanced Materials* **2013**, *25*, 4245-4266.

22. An, Q.; Zhang, F.; Zhang, J.; Tang, W.; Deng, Z.; Hu, B. Versatile ternary organic solar cells: A critical review. *Energy Environ. Sci.* **2015**, *9*, doi:10.1039/C5EE02641E.
23. Bi, P.; Hao, X. Versatile ternary approach for novel organic solar cells: a review. *Solar RRL* **2019**, *3*, 1800263.
24. Gasparini, N.; Salleo, A.; McCulloch, I.; Baran, D. The role of the third component in ternary organic solar cells. *Nature Reviews Materials* **2019**, *4*, 229-242, doi:10.1038/s41578-019-0093-4.
25. Chang, L.; Sheng, M.; Duan, L.; Uddin, A. Ternary organic solar cells based on non-fullerene acceptors: A review. *Organic Electronics* **2021**, *90*, 106063, doi:https://doi.org/10.1016/j.orgel.2021.106063.
26. Jhuo, H.-J.; Yeh, P.-N.; Liao, S.-H.; Li, Y.-L.; Cheng, Y.-S.; Chen, S.-A. Review on the Recent Progress in Low Band Gap Conjugated Polymers for Bulk Hetero-junction Polymer Solar Cells. *Journal of the Chinese Chemical Society* **2014**, *61*, 115-126, doi:https://doi.org/10.1002/jccs.201300333.
27. Zhang, X.; Wang, Q.; Shen, W.; Han, C.; Shao, Y.; Belfiore, L.A.; Tang, J. Recent advances and prospects of D1:D2:A non-fullerene ternary polymer solar cells. *Journal of Materials Chemistry C* **2021**, *9*, 41-66, doi:10.1039/D0TC04407E.
28. Zhao, Y.; Zhu, Y.; Cheng, H.-W.; Zheng, R.; Meng, D.; Yang, Y. A review on semitransparent solar cells for agricultural application. *Materials Today Energy* **2021**, *22*, 100852.
29. Brus, V.V.; Lee, J.; Luginbuhl, B.R.; Ko, S.J.; Bazan, G.C.; Nguyen, T.Q. Solution-Processed Semitransparent Organic Photovoltaics: From Molecular Design to Device Performance. *Advanced Materials* **2019**, *31*, 1900904.
30. Dai, S.; Zhan, X. Nonfullerene acceptors for semitransparent organic solar cells. *Advanced Energy Materials* **2018**, *8*, 1800002.
31. Duan, L.; Hoex, B.; Uddin, A. Progress in Semitransparent Organic Solar Cells. *Solar RRL* **2021**, *5*, 2100041, doi:https://doi.org/10.1002/solr.202100041.
32. Zhu, F. Semitransparent Organic Solar Cells. *Frontiers of Optoelectronics* **2014**, *7*, 20-27, doi:10.1007/s12200-014-0395-5.
33. Hu, Z.; Wang, J.; Ma, X.; Gao, J.; Xu, C.; Yang, K.; Wang, Z.; Zhang, J.; Zhang, F. A critical review on semitransparent organic solar cells. *Nano Energy* **2020**, *78*, 105376, doi:https://doi.org/10.1016/j.nanoen.2020.105376.
34. Han, S.; Deng, Y.; Han, W.; Ren, G.; Song, Z.; Liu, C.; Guo, W. Recent advances of semitransparent organic solar cells. *Solar Energy* **2021**, *225*, 97-107, doi:https://doi.org/10.1016/j.solener.2021.06.068.
35. Kini, G.P.; Jeon, S.J.; Moon, D.K. Latest Progress on Photoabsorbent Materials for Multifunctional Semitransparent Organic Solar Cells. *Advanced Functional Materials* **2021**, *31*, 2007931, doi:https://doi.org/10.1002/adfm.202007931.
36. Khandelwal, K.; Biswas, S.; Mishra, A.; Sharma, G.D. Semitransparent organic solar cells: from molecular design to structure–performance relationships. *Journal of Materials Chemistry C* **2022**, *10*, 13-43, doi:10.1039/D1TC04569E.
37. Yao, N.; Xia, Y.; Liu, Y.; Chen, S.; Jonsson, M.P.; Zhang, F. Solution-Processed Highly Efficient Semitransparent Organic Solar Cells with Low Donor Contents. *ACS Applied Energy Materials* **2021**, *4*, 14335-14341, doi:10.1021/acsaem.1c03017.
38. Sano, T.; Inaba, S.; Vohra, V. Ternary Active Layers for Neutral Color Semitransparent Organic Solar Cells with PCEs over 4%. *ACS Applied Energy Materials* **2019**, *2*, 2534-2540, doi:10.1021/acsaem.8b02144.
39. Rahim, B.K.; Amin, P.O.; Muhammadsharif, F.F.; Saeed, S.R.; Ketuly, K.A. Optical and Optoelectronic Studies of Binary and Ternary Films of Poly (L-Tryptophane), Poly (5-hydroxy-L-tryptophane), and P (TER-CO-TRI) Doped with Sudan Dye. *ARO-THE SCIENTIFIC JOURNAL OF KOYA UNIVERSITY* **2023**, *11*, 105-115.
40. Zhang, G.; Zhao, J.; Chow, P.C.Y.; Jiang, K.; Zhang, J.; Zhu, Z.; Zhang, J.; Huang, F.; Yan, H. Nonfullerene Acceptor Molecules for Bulk Heterojunction Organic Solar Cells. *Chemical Reviews* **2018**, *118*, 3447-3507, doi:10.1021/acs.chemrev.7b00535.
41. Koppe, M.; Egelhaaf, H.-J.; Clodic, E.; Morana, M.; Lüer, L.; Troeger, A.; Sgobba, V.; Guldi, D.M.; Ameri, T.; Brabec, C.J. Charge Carrier Dynamics in a Ternary Bulk Heterojunction System Consisting of P3HT, Fullerene, and a Low Bandgap Polymer. *Advanced Energy Materials* **2013**, *3*, 949-958, doi:https://doi.org/10.1002/aenm.201201076.
42. Honda, S.; Ohkita, H.; Benten, H.; Ito, S. Selective Dye Loading at the Heterojunction in Polymer/Fullerene Solar Cells. *Advanced Energy Materials* **2011**, *1*, 588-598, doi:https://doi.org/10.1002/aenm.201100094.
43. Koppe, M.; Egelhaaf, H.-J.; Dennler, G.; Scharber, M.C.; Brabec, C.J.; Schilinsky, P.; Hoth, C.N. Near IR Sensitization of Organic Bulk Heterojunction Solar Cells: Towards Optimization of the Spectral Response of Organic Solar Cells. *Advanced Functional Materials* **2010**, *20*, 338-346, doi:https://doi.org/10.1002/adfm.200901473.
44. Zhang, M.; Wang, J.; Zhang, F.; Mi, Y.; An, Q.; Wang, W.; Ma, X.; Zhang, J.; Liu, X. Ternary small molecule solar cells exhibiting power conversion efficiency of 10.3%. *Nano Energy* **2017**, *39*, 571-581, doi:https://doi.org/10.1016/j.nanoen.2017.07.044.

45. Jones, G.A.; Bradshaw, D.S. Resonance Energy Transfer: From Fundamental Theory to Recent Applications. *Frontiers in Physics* **2019**, *7*, doi:10.3389/fphy.2019.00100.
46. Löslein, H.; Ameri, T.; Matt, G.J.; Koppe, M.; Egelhaaf, H.J.; Troeger, A.; Sgobba, V.; Guldi, D.M.; Brabec, C.J. Transient absorption spectroscopy studies on polythiophene-fullerene bulk heterojunction organic blend films sensitized with a low-bandgap polymer. *Macromol Rapid Commun* **2013**, *34*, 1090-1097, doi:10.1002/marc.201300354.
47. Street, R.A.; Davies, D.; Khlyabich, P.P.; Burkhart, B.; Thompson, B.C. Origin of the Tunable Open-Circuit Voltage in Ternary Blend Bulk Heterojunction Organic Solar Cells. *Journal of the American Chemical Society* **2013**, *135*, 986-989, doi:10.1021/ja3112143.
48. Yang, L.; Zhou, H.; Price, S.C.; You, W. Parallel-like bulk heterojunction polymer solar cells. *Journal of the American Chemical Society* **2012**, *134*, 5432-5435.
49. Hossain, N.; Das, S.; Alford, T. Equivalent Circuit Modification for Organic Solar Cells. *Circuits and Systems* **2015**, *06*, 153-160, doi:10.4236/cs.2015.66016.
50. Cheknane, A.; Hilal, H.S.; Djeffal, F.; Benyoucef, B.; Charles, J.-P. An equivalent circuit approach to organic solar cell modelling. *Microelectronics Journal* **2008**, *39*, 1173-1180, doi:https://doi.org/10.1016/j.mejo.2008.01.053.
51. Abdulkarim, Y.I.; Deng, L.; Muhammad, F.F.; He, L. Enhanced light absorption in the organic thin films by coating cross-shaped metamaterial resonators onto the active layers. *Results in Physics* **2019**, *13*, 102338, doi:https://doi.org/10.1016/j.rinp.2019.102338.
52. Reference Air Mass 1.5 Spectra. Available online: https://www.nrel.gov/grid/solar-resource/spectra-am1.5.html (accessed on November).
53. Liu, J.; Chen, S.; Qian, D.; Gautam, B.; Yang, G.; Zhao, J.; Bergqvist, J.; Zhang, F.; Ma, W.; Ade, H.; et al. Fast charge separation in a non-fullerene organic solar cell with a small driving force. *Nature Energy* **2016**, *1*, 16089, doi:10.1038/nenergy.2016.89.
54. Basic Characteristics and Characterization of Solar Cells. In *Materials Concepts for Solar Cells*; WORLD SCIENTIFIC (EUROPE): 2017; pp. 3-43.
55. Proctor, C.M.; Kuik, M.; Nguyen, T.-Q. Charge carrier recombination in organic solar cells. *Progress in Polymer Science* **2013**, *38*, 1941-1960, doi:https://doi.org/10.1016/j.progpolymsci.2013.08.008.
56. Ameri, T.; Dennler, G.; Waldauf, C.; Azimi, H.; Seemann, A.; Forberich, K.; Hauch, J.; Scharber, M.; Hingerl, K.; Brabec, C.J. Fabrication, Optical Modeling, and Color Characterization of Semitransparent Bulk-Heterojunction Organic Solar Cells in an Inverted Structure. *Advanced Functional Materials* **2010**, *20*, 1592-1598, doi:https://doi.org/10.1002/adfm.201000176.
57. Alqurashy, B.A.; Iraqi, A.; Zhang, Y.; Lidzey, D.G. Pyrene-benzo [1,2,5]thiadiazole based conjugated polymers for application in BHJ solar cells. *Journal of Saudi Chemical Society* **2020**, *24*, 484-491, doi:https://doi.org/10.1016/j.jscs.2020.04.004.
58. Kim, J.; Chae, S.; Yi, A.; Hong, S.; Kim, H.J.; Suh, H. Characterization of push-pull type of conjugated polymers containing 8H-thieno [2,3-b]indole for organic photovoltaics. *Synthetic Metals* **2018**, *245*, 267-275, doi:https://doi.org/10.1016/j.synthmet.2018.09.018.
59. Muhammad, F.F.; Yahya, M.Y.; Aziz, F.; Rasheed, M.A.; Sulaiman, K. Tuning the extinction coefficient, refractive index, dielectric constant and optical conductivity of Gaq3 films for the application of OLED displays technology. *Journal of Materials Science: Materials in Electronics* **2017**, *28*, 14777-14786, doi:10.1007/s10854-017-7347-y.
60. Tauc, J. Optical properties and electronic structure of amorphous Ge and Si. *Materials Research Bulletin* **1968**, *3*, 37-46.
61. Song, Q.; Li, F.; Wang, Z.; Zhang, X. A supramolecular strategy for tuning the energy level of naphthalenediimide: Promoted formation of radical anions with extraordinary stability. *Chemical science* **2015**, *6*, 3342-3346.
62. Muhammad, F.F.; Sulaiman, K. Utilizing a simple and reliable method to investigate the optical functions of small molecular organic films – Alq3 and Gaq3 as examples. *Measurement* **2011**, *44*, 1468-1474, doi:https://doi.org/10.1016/j.measurement.2011.05.017.
63. Davis, E.; Mott, N. Conduction in non-crystalline systems V. Conductivity, optical absorption and photoconductivity in amorphous semiconductors. *Philosophical Magazine* **1970**, *22*, 0903-0922.
64. Cardona, C.M.; Li, W.; Kaifer, A.E.; Stockdale, D.; Bazan, G.C. Electrochemical considerations for determining absolute frontier orbital energy levels of conjugated polymers for solar cell applications. *Advanced materials* **2011**, *23*, 2367-2371.
65. Mdluli, S.B.; Ramoroka, M.E.; Yussuf, S.T.; Modibane, K.D.; John-Denk, V.S.; Iwuoha, E.I. π-Conjugated Polymers and Their Application in Organic and Hybrid Organic-Silicon Solar Cells. *Polymers* **2022**, *14*, 716.
66. Gurney, R.S.; Lidzey, D.G.; Wang, T. A review of non-fullerene polymer solar cells: from device physics to morphology control. *Reports on Progress in Physics* **2019**, *82*, 036601, doi:10.1088/1361-6633/ab0530.

67. Dang, M.T.; Wantz, G.; Bejbouji, H.; Urien, M.; Dautel, O.J.; Vignau, L.; Hirsch, L. Polymeric solar cells based on P3HT:PCBM: Role of the casting solvent. *Solar Energy Materials and Solar Cells* **2011**, *95*, 3408-3418, doi:https://doi.org/10.1016/j.solmat.2011.07.039.
68. Çetinkaya, Ç.; Çokduygulular, E.; Kınacı, B.; Güzelçimen, F.; Özen, Y.; Efkere, H.İ.; Candan, İ.; Emik, S.; Özçelik, S. Design and fabrication of a semi-transparent solar cell considering the effect of the layer thickness of MoO3/Ag/MoO3 transparent top contact on optical and electrical properties. *Scientific Reports* **2021**, *11*, 13079, doi:10.1038/s41598-021-92539-8.
69. Bliznyuk, V.N.; Gasiorowski, J.; Ishchenko, A.A.; Bulavko, G.V.; Rahaman, M.; Hingerl, K.; Zahn, D.R.T.; Sariciftci, N.S. Photovoltaic cells based on ternary P3HT:PCBM:polymethine dye active layer transparent in the visible range of light. *Applied Surface Science* **2016**, *389*, 419-427, doi:https://doi.org/10.1016/j.apsusc.2016.07.130.
70. Yuanpeng, X.; Huo, L.; Fan, B.; Fu, H.; Cai, Y.; Zhang, L.; Li, Z.; Wang, Y.; Ma, W.; Chen, Y.; et al. High-Performance Semitransparent Ternary Organic Solar Cells. *Advanced Functional Materials* **2018**, *28*, 1800627, doi:10.1002/adfm.201800627.
71. Liu, W.; Sun, S.; Zhou, L.; Cui, Y.; Zhang, W.; Hou, J.; Liu, F.; Xu, S.; Zhu, X. Design of Near-Infrared Nonfullerene Acceptor with Ultralow Nonradiative Voltage Loss for High-Performance Semitransparent Ternary Organic Solar Cells. *Angewandte Chemie International Edition* **2021**, *n/a*, e202116111, doi:https://doi.org/10.1002/anie.202116111.
72. Zhou, K.; Xian, K.; Ye, L. Morphology control in high-efficiency all-polymer solar cells. *InfoMat* **2022**, *4*, e12270, doi:https://doi.org/10.1002/inf2.12270.
73. Lu, H.; Li, M.; Bi, Z.; Gong, X.; Li, G.; Feng, S.; Xu, X.; Ma, W.; Bo, Z. Using ternary blend as a strategy to improve the driving force for charge transfer and facilitate electron transport in polymer solar cells. *Organic Electronics* **2019**, *65*, 419-425, doi:https://doi.org/10.1016/j.orgel.2018.11.040.
74. Liu, J.; Yin, Y.; Wang, K.; Wei, P.; Lu, H.; Song, C.; Liang, Q.; Huang, W. Domain size control in all-polymer solar cells. *iScience* **2022**, *25*, 104090, doi:https://doi.org/10.1016/j.isci.2022.104090.
75. Ke, L.; Min, J.; Adam, M.; Gasparini, N.; Hou, Y.; Perea, J.D.; Chen, W.; Zhang, H.; Fladischer, S.; Sale, A.-C.; et al. A Series of Pyrene-Substituted Silicon Phthalocyanines as Near-IR Sensitizers in Organic Ternary Solar Cells. *Advanced Energy Materials* **2016**, *6*, 1502355, doi:https://doi.org/10.1002/aenm.201502355.
76. Stylianakis, M.M.; Konios, D.; Viskadouros, G.; Vernardou, D.; Katsarakis, N.; Koudoumas, E.; Anastasiadis, S.H.; Stratakis, E.; Kymakis, E. Ternary organic solar cells incorporating zinc phthalocyanine with improved performance exceeding 8.5%. *Dyes and Pigments* **2017**, *146*, 408-413, doi:https://doi.org/10.1016/j.dyepig.2017.07.032.
77. Zhang, M.; Zhang, F.; An, Q.; Sun, Q.; Wang, J.; Li, L.; Wang, W.; Zhang, J. High efficient ternary polymer solar cells based on absorption complementary materials as electron donor. *Solar Energy Materials and Solar Cells* **2015**, *141*, 154-161, doi:https://doi.org/10.1016/j.solmat.2015.05.037.
78. Makha, M.; Testa, P.; Anantharaman, S.B.; Heier, J.; Jenatsch, S.; Leclaire, N.; Tisserant, J.-N.; Véron, A.C.; Wang, L.; Nüesch, F.; et al. Ternary semitransparent organic solar cells with a laminated top electrode. *Science and Technology of Advanced Materials* **2017**, *18*, 68-75, doi:10.1080/14686996.2016.1261602.
79. Min, J.; Ameri, T.; Gresser, R.; Lorenz-Rothe, M.; Baran, D.; Troeger, A.; Sgobba, V.; Leo, K.; Riede, M.; Guldi, D.M.; et al. Two Similar Near-Infrared (IR) Absorbing Benzannulated Aza-BODIPY Dyes as Near-IR Sensitizers for Ternary Solar Cells. *ACS Applied Materials & Interfaces* **2013**, *5*, 5609-5616, doi:10.1021/am400923b.
80. Vohra, V.; Uchiyama, T.; Inaba, S.; Okada-Shudo, Y. Efficient ultrathin organic solar cells with sustainable β-carotene as electron donor. *ACS Sustainable Chemistry & Engineering* **2019**, *7*, 4376-4381.
81. Duan, S.; Zhou, Q.; Dall'Agnese, C.; Chen, G.; Wang, X.-F.; Tamiaki, H.; Sakai, K.; Ikeuchi, T.; Sasaki, S.-i. Organic Solar Cells Based on the Aggregate of Synthetic Chlorophyll Derivative with over 5% Efficiency. *Solar RRL* **2019**, *3*, 1900203, doi:https://doi.org/10.1002/solr.201900203.
82. Wang, Y.; Zhuang, C.; Fang, Y.; Yu, H.; Wang, B. Various roles of dye molecules in organic ternary blend solar cells. *Dyes and Pigments* **2020**, *176*, 108231, doi:https://doi.org/10.1016/j.dyepig.2020.108231.
83. Vohra, V. Natural Dyes and Their Derivatives Integrated into Organic Solar Cells. *Materials* **2018**, *11*, 2579.
84. Li, M.; Li, N.; Chen, G.; Sasaki, S.-i.; Miyasaka, T.; Tamiaki, H.; Dall'Agnese, C.; Wang, X.-F. Perovskite solar cells based on chlorophyll hole transporters: Dependence of aggregation and photovoltaic performance on aliphatic chains at C17-propionate residue. *Dyes and Pigments* **2019**, *162*, 763-770, doi:https://doi.org/10.1016/j.dyepig.2018.11.005.
85. Li, Y.; Huang, W.; Zhao, D.; Wang, L.; Jiao, Z.; Huang, Q.; Wang, P.; Sun, M.; Yuan, G. Recent Progress in Organic Solar Cells: A Review on Materials from Acceptor to Donor. *Molecules* **2022**, *27*, 1800.
86. Chen, J.; Chen, Y.; Feng, L.-W.; Gu, C.; Li, G.; Su, N.; Wang, G.; Swick, S.M.; Huang, W.; Guo, X.; et al. Hole (donor) and electron (acceptor) transporting organic semiconductors for bulk-heterojunction solar cells. *EnergyChem* **2020**, *2*, 100042, doi:https://doi.org/10.1016/j.enchem.2020.100042.

87. Wang, X.; Zhai, X.; Jing, X.; Gao, C.; He, Y.; Yu, L.; Sun, M. Incorporation of a classical visible non-fullerene acceptor into host binary blend enable ternary high-performance semitransparent polymer solar cells. *Chemical Engineering Journal* **2022**, *427*, 132048, doi:https://doi.org/10.1016/j.cej.2021.132048.
88. Liu, Y.; Yan, Y.; Zhang, Q.; Zhang, J.; Yu, X.; Han, Y. Increasing the nucleation and growth barrier of a non-fullerene acceptor to achieve bicontinuous pathways in semitransparent ternary polymer solar cells. *Journal of Materials Chemistry C* **2021**, *9*, 5713-5722, doi:10.1039/D1TC00691F.
89. Xie, Y.; Huo, L.; Fan, B.; Fu, H.; Cai, Y.; Zhang, L.; Li, Z.; Wang, Y.; Ma, W.; Chen, Y.; et al. High-Performance Semitransparent Ternary Organic Solar Cells. *Advanced Functional Materials* **2018**, *28*, 1800627, doi:https://doi.org/10.1002/adfm.201800627.
90. Wang, X.; Zhai, X.; Kang, X.; Ding, X.; Gao, C.; Jing, X.; Yu, L.; Sun, M. High-Performance Ternary Semitransparent Polymer Solar Cells with Different Bandgap Third Component as Non-Fullerene Guest Acceptor. *Solar RRL* **2022**, *n/a*, 2200070, doi:https://doi.org/10.1002/solr.202200070.
91. Zhang, Y.; Luo, D.; Shan, C.; Liu, Q.; Gu, X.; Li, W.; Choy, W.C.H.; Kyaw, A.K.K. High-Performance Semitransparent Organic Solar Cells Enabled by Improved Charge Transport and Optical Engineering of Ternary Blend Active Layer. *Solar RRL* **2022**, *6*, 2100785, doi:https://doi.org/10.1002/solr.202100785.
92. Lu, X.; Cao, L.; Du, X.; Lin, H.; Zheng, C.; Chen, Z.; Sun, B.; Tao, S. Hydrogen-Bond-Induced High Performance Semitransparent Ternary Organic Solar Cells with 14% Efficiency and Enhanced Stability. *Advanced Optical Materials* **2021**, *9*, 2100064, doi:10.1002/adom.202100064.
93. Hu, Z.; Wang, J.; Wang, Z.; Gao, W.; An, Q.; Zhang, M.; Ma, X.; Wang, J.; Miao, J.; Yang, C.; et al. Semitransparent Ternary Nonfullerene Polymer Solar Cells Exhibiting 9.40% Efficiency and 24.6% Average Visible Transmittance. *Nano Energy* **2018**, *55*, doi:10.1016/j.nanoen.2018.11.010.
94. Jiang, T.; Zhang, G.; Xia, R.; Huang, J.; Li, X.; Wang, M.; Yip, H.L.; Cao, Y. Semitransparent organic solar cells based on all-low-bandgap donor and acceptor materials and their performance potential. *Materials Today Energy* **2021**, *21*, 100807, doi:https://doi.org/10.1016/j.mtener.2021.100807.
95. Yin, P.; Yin, Z.; Ma, Y.; Zheng, Q. Improving the charge transport of the ternary blend active layer for efficient semitransparent organic solar cells. *Energy & Environmental Science* **2020**, *13*, 5177-5185, doi:10.1039/D0EE03378B.
96. Hu, Z.; Wang, J.; Ma, X.; Jinhua, G.; Xu, C.; Wang, X.; Zhang, X.; Wang, Z.; Zhang, F. Semitransparent organic solar cells exhibiting 13.02% efficiency and 20.2% average visible transmittance. *Journal of Materials Chemistry A* **2021**, *9*, doi:10.1039/D1TA01135A.
97. Cheng, P.; Wang, H.-C.; Zhu, Y.; Zheng, R.; Li, T.; Chen, C.-H.; Huang, T.; Zhao, Y.; Wang, R.; Meng, D.; et al. Transparent Hole-Transporting Frameworks: A Unique Strategy to Design High-Performance Semitransparent Organic Photovoltaics. *Advanced Materials* **2020**, *32*, doi:10.1002/adma.202003891.
98. Zhang, J.; Xu, G.; Tao, F.; Zeng, G.; Zhang, M.; Yang, Y.; Li, Y.; Li, Y. Highly Efficient Semitransparent Organic Solar Cells with Color Rendering Index Approaching 100. *Advanced Materials* **2019**, *31*, 1807159, doi:https://doi.org/10.1002/adma.201807159.
99. Wang, D.; Qin, R.; Zhou, G.; Li, X.; Xia, R.; Li, Y.; Zhan, L.; Zhu, H.; Lu, X.; Yip, H.-L.; et al. High-Performance Semitransparent Organic Solar Cells with Excellent Infrared Reflection and See-Through Functions. *Advanced Materials* **2020**, *32*, 2001621, doi:https://doi.org/10.1002/adma.202001621.
100. Zhang, Y.; Luo, D.; Shan, C.; Liu, Q.; Gu, X.; Li, W.; Choy, W.; Kyaw, A. High-Performance Semitransparent Organic Solar Cells Enabled by Improved Charge Transport and Optical Engineering of Ternary Blend Active Layer. *Solar RRL* **2021**, *6*, doi:10.1002/solr.202100785.
101. Tang, H.; Wu, J.; Liu, H.; Wang, B.; Wang, H.; Li, Y.; Fu, Y.; Xie, Z. Semi-transparent organic solar cells with high visible transmission enabled by a transparent wide-bandgap donor. *Organic Electronics* **2021**, *93*, 106140, doi:10.1016/j.orgel.2021.106140.
102. Chen, C.-C.; Dou, L.; Zhu, R.; Chung, C.-H.; Song, T.-B.; Zheng, Y.B.; Hawks, S.; Li, G.; Weiss, P.S.; Yang, Y. Visibly transparent polymer solar cells produced by solution processing. *ACS nano* **2012**, *6*, 7185-7190.
103. Ji, G.; Wang, Y.; Luo, Q.; Han, K.; Xie, M.; Zhang, L.; Wu, N.; Lin, J.; Xiao, S.; Li, Y.-Q.; et al. Fully Coated Semitransparent Organic Solar Cells with a Doctor-Blade-Coated Composite Anode Buffer Layer of Phosphomolybdic Acid and PEDOT:PSS and a Spray-Coated Silver Nanowire Top Electrode. *ACS Applied Materials & Interfaces* **2018**, *10*, 943-954, doi:10.1021/acsami.7b13346.
104. Maisch, P.; Tam, K.C.; Lucera, L.; Egelhaaf, H.-J.; Scheiber, H.; Maier, E.; Brabec, C.J. Inkjet printed silver nanowire percolation networks as electrodes for highly efficient semitransparent organic solar cells. *Organic Electronics* **2016**, *38*, 139-143, doi:https://doi.org/10.1016/j.orgel.2016.08.006.
105. Sannicolo, T.; Chae, W.H.; Mwaura, J.; Bulović, V.; Grossman, J.C. Silver Nanowire Back Electrode Stabilized with Graphene Oxide Encapsulation for Inverted Semitransparent Organic Solar Cells with Longer Lifetime. *ACS Applied Energy Materials* **2021**, *4*, 1431-1441, doi:10.1021/acsaem.0c02639.
106. Schmidt, H.; Flügge, H.; Winkler, T.; Bülow, T.; Riedl, T.; Kowalsky, W. Efficient semitransparent inverted organic solar cells with indium tin oxide top electrode. *Applied Physics Letters* **2009**, *94*, 243302, doi:10.1063/1.3154556.

107. Huang, J.; Li, G.; Yang, Y. A Semi-transparent Plastic Solar Cell Fabricated by a Lamination Process. *Advanced Materials* **2008**, *20*, 415-419, doi:https://doi.org/10.1002/adma.200701101.